communications earth & environment

ARTICLE

https://doi.org/10.1038/s43247-023-01129-1 OPEN

A multi-sensor approach for increased measurements of floods and their societal impacts from space

Dinuke Munasinghe [1✉], Renato Prata de Moraes Frasson [1], Cédric H. David [1], Matthew Bonnema[1], Guy Schumann [2,3] & G. Robert Brakenridge [4]

Merging observations from multiple satellites is necessary to ensure that extreme hydrological events are consistently observed. Here, we evaluate the potential improvements to flood detectability afforded by combining data collected globally by Landsat, Sentinel-2, and Sentinel-1. The enhanced temporal sampling increased the number of floods with at least 1 useful image (≤20% clouds) from 7% for single sensors to up to 66% for a potential multi-sensor product. As dramatic as the increased coverage is, the socioeconomic impacts are even more tangible. In the pre-Sentinel era, only 22% of the total population displaced by flood events benefitted from having high-resolution images, whereas a potential multi-sensor product would serve 75% of the displaced population. Additionally, the merged dataset could observe up to 100% of floods caused by challenging drivers, e.g., tropical cyclones, tidal surges, including those rarely seen by single sensors, and thereby enable insights into governing mechanisms of these events.

[1] Jet Propulsion Laboratory, California Institute of Technology, Pasadena, CA, USA. [2] School of Geographical Sciences, University of Bristol, Bristol, UK. [3] Research and Education Department, RSS-Hydro, Kayl, Luxembourg. [4] INSTAAR, Dartmouth Flood Observatory, University of Colorado, Boulder, CO, USA. ✉email: dinukem@jpl.nasa.gov

Flooding is the deadliest and costliest natural disaster, both in the US and worldwide. It devastates cities, farmlands, and infrastructure, causes the loss of human lives, and contributes to disease outbreaks and reductions in food and water security[1]. Global damages due to flooding since 1980 exceed $1 trillion[2] and by the end of the century, it is estimated that climate change will increase these losses by up to a factor of 20[3]. Mapping extents and impacts of flood events in near-real time is of utmost importance for first responders, whereas long-term observations are instrumental for policymakers, government agencies, and insurance companies for quantifying flood risks. Disaster management teams need accurate flood information to assess impacted areas to quantify damage, coordinate mitigation efforts, and determine insurance refunds. Additionally, scientists rely on flood information—by using flooded area as a metric—to calibrate prediction models to assess model performance for future risk assessment and management[4].

Earth-observing satellites have become a strong asset in investigations of global floods[5–7]. They provide large amounts of worldwide or near-worldwide data, can fill data gaps in the existing network of stream gauges[8–10], cover geographical locations inaccessible to humans, and circumvent restrictions on data sharing across country borders[11–13]. However, one of the major limitations is the sparse temporal sampling afforded by many satellite missions.

The typical time between observations, ranging from days to weeks, may lead to loss of crucial flood information, and at times leave flood events with no imagery at all. The uneven spatial and temporal sampling produced by the new wide-swath altimeter of the Surface Water and Ocean Topography (SWOT) mission is likely to miss a significant portion (~45%) of globally occurring floods[14]. Traditional nadir altimeters also did not fare much better; space and time samplings of these missions are limited in their ability to observe floods that last few days or less[15], and global distributions of extreme discharge values (typically leading to floods) required more frequent sampling for accurate detection[16]. For example, not every ephemeral flood that peaked and retreated over the Murray–Darling Basin, Australia could be captured by Landsat TM/ETM+[17].

There is currently widespread recognition of the need for better observations and quantification of surface water and flooding dynamics[18]. The frequency of sampling is increased when data from several missions are combined or a constellation of satellites is used, which is needed as no single orbit produces samples with adequate spatial coverage and temporal resolution[15]. The increased temporal sampling is also helpful in reducing the possibility that any place of interest may have data gaps from cloud cover (optical) or high attenuation from heavy rain (radar). Additionally, the short revisit period afforded by mission architecture based on constellations of satellites or by multi-mission merging increases the number of available images per event, which translates to better imagery (i.e., more stringent quality controls on imagery increases the ability to observe flood dynamics).

For the Murray-Darling Basin, merging of Landsat and Sentinel-2 imagery by Harmonized Landsat and Sentinel-2 (HLS) detected more ephemeral flooding compared to Landsat-8 and Sentinel-2, individually[17]. The improved effectiveness of combined Sentinel-1 and Sentinel-2 to map floods in Europe based on the revisit time of the satellite constellations and the presence of atmospheric clouds has also been demonstrated[7]. Inundation extent measurements from visible (Landsat-8 and Sentinel-2) and SAR (Sentinel-1) imagery were compared and contrasted for selected water bodies in Bangladesh for the monsoonal/post-monsoonal time period[19]. Additional work has demonstrated the benefits of multi-mission merging for measuring flood duration[20]. Here we evaluate, on a global scale, the benefits of combination of three families of satellite missions (Landsat, Sentinel-2 and Sentinel-1) to quantify the increased detection of floods caused by different drivers, including tropical cyclones, ice jams/breakups, and others. We also assess the potential societal benefits of the finer spatiotemporal sampling afforded by multi-sensor combination by quantifying the number of displaced people with and without access to high-resolution spatial imagery obtained during the flood events, as inundation maps produced from such imagery may be used for disaster response, recovery, and to support actions to increase flood resilience.

Our goals are to: first, compare the flood detection potential between individual sensors and the combination of satellite sensors. This is achieved by calculating global revisit periods at a 0.5° grid resolution for the sensor(s), and then, comparing the durations of historical floods to the revisit times at the flood location on the 0.5° resolution grid. Second, we wish to understand the upper limit and lower limit of image availability for global floods between single sensor vs their combination over time. The upper limit assumes that all captured imagery could be used for flood information (e.g., extent, depth) extraction, whereas the lower limit accounts for data quality by setting a cloud cover threshold for image viability (≤20% atmospheric cloud cover threshold). This is obtained by quantifying the availability of imagery for 5130 media-reported historical flood events since 1985. The detection limits are compared and contrasted between single and combined sensors. Finally, we demonstrate how the increase in viable imagery leads to the identification of different drivers of global floods (i.e., monsoonal rain-driven, dam break-driven) and estimate how the more frequent revisit times serve the affected human populations. This is achieved by quantifying the different drivers of floods captured by the combination of sensors compared to single sensors, and quantifying the number of flood events that displaced human populations and for which remotely sensed imagery was available.

Results

Global revisit periods of satellites and their flood detection potential. The global revisit periods of the different sensor platforms are shown in Fig. 1a1–a4. The 'revisit period' is the mean time elapsed between observations of the same point on Earth by a satellite. In contrast, the 'repeat cycle' is the time elapsed between nadir points of satellite passes over the same point when the satellite retraces its path. Revisit periods can be smaller than repeat cycles due to swath overlaps. Average revisit periods of the three satellite missions and their combination were enumerated at a 0.5° global grid spacing based on imagery acquired (regardless of image quality) between 2016 and 2020. Details on the rationale for a 0.5° grid, constructing the global grid, the choice of multiple years to calculate an 'average revisit period', and calculating revisit periods for each of the grid points for the 3 missions (5 satellites; Landsat-8, Sentinel-1 twin satellites, Sentinel-2 twin satellites) can be found in the Methods section.

As expected, we find that leveraging different data sources leads to a combined spatiotemporal sampling that is better than any single sensor and results in a much-increased capture of global floods. The global median revisit period ranges from 12.3 days for Landsat (Figs. 1a1); 12.0 days for Sentinel-1 (Figs. 1a2), 4.2 days for Sentinel-2 (Figs. 1a3) to only 2.4 days, for the composite evaluation of the three sensors together (Fig. 1a4). This is a frequency increase of 80.5% for the composite of satellites compared to the individual sensor system with the highest revisit time (Landsat, at 12.3 days). In the composite (Fig. 1a4), the northern Latitudes (70°−85°) show median revisit periods as low as 0.7 days, the tropical region (latitudes 23.5° N–23.5° S), 3.4 days, and the lower latitudes (40° S − 60° S) 2.2 days, a

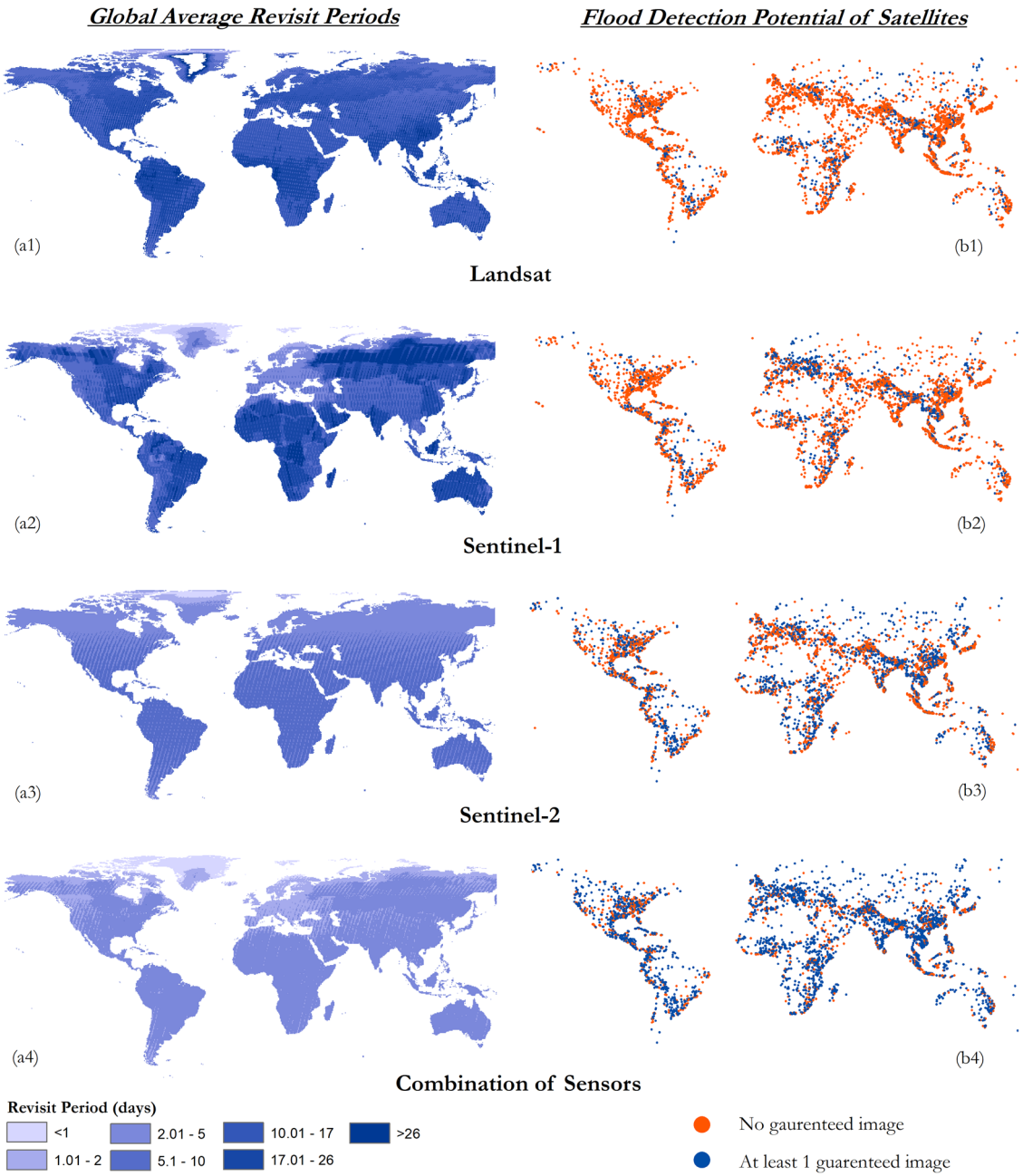

Fig. 1 The potential for flood detection by different missions based on average global revisit periods. a1–a4 Global revisit periods of individual missions and their combination. **b1–b4** Potential detection of DFO floods by the sensors if sensors were operational at the time of each event. Flood events with at least 1 guaranteed image (flood duration > revisit period at flood centroid location) are depicted in blue: no guaranteed images, in orange. The striping pattern (A1-A4) results from satellite swath overlap resulting in high frequency sampling in overlapping areas. Downlink restrictions on Sentinel-1 imagery cause relatively low observation frequencies in northern Russia and Mongolia.

considerable improvement from 7, 16.8 and 9.8 days for Landsat for the same latitudinal belts, respectively. We also find that certain regions (i.e., South America, China and Eastern Africa) are observation-poor when only Landsat is considered (due to downlink limitations that may cause operators to prioritize geographical areas, spacecraft maneuvers to balance heat, orbit corrections, and sensor malfunctions), but observations greatly increase in spatial coverage when the individual sensor results are combined. The improvements in South America and Eastern Africa especially are attributed to the addition of Sentinel-2 and its better revisit times in these areas.

Comparing the revisit period with the duration of a flood event allows a metric for measuring the potential for flood detection by a satellite/group of satellites. We contrast the temporal sampling of the individual missions and the potential merged product with the flood durations of 5130 reported events in the DFO (Dartmouth Flood Observatory) database[21]. We assume that floods with durations greater than the revisit period of the satellite in consideration, or the group of satellites, at the location of each flood would have a guaranteed observation if the satellite mission(s) was operational at the time of the event. Conversely, if the duration of the flood was smaller than the revisit period, that event would only be observed by chance, depending on how the event duration aligned with the data acquisition times. The observed improvement in revisit periods is reflected in the floods that would have been captured by different missions as shown in

Fig. 1b1–b4). For comparison purposes, we assume that all 3 missions were operational since 1985 (the earliest date of a flood record in the DFO database). By comparing the revisit periods of the satellite missions with the duration of flood events, we find that if Landsat were the only operational platform at the time of the events, out of the 5130 floods in the database, only 19.1% would have had a guaranteed observation (Figs. 1b1). Over 80% of the floods were not guaranteed an image acquisition (only a fortuitous acquisition would have been possible). For Sentinel-1 and 2, the fraction of events with guaranteed acquisitions were 27.9% and 46.6% respectively (Figs. 1b2/b3). Using the same criteria, the composite shows detection of at least 72.0% of global floods, not including events with fortuitous acquisition (Fig. 1b4).

How well are floods captured over time? Next, we consider the potential for flood capture by the sensors as compared to location-averaged (grid-based) return periods. We empirically evaluated the existence of images during the floods for the 5130 historical events in the DFO database. This event-based enumeration accounts for irregular revisit periods of satellites, image downlink issues, and other random download interruptions not reflected in the average revisit time calculations, and it provides the exact availability of imagery per flood event. For each year since 1985, we tabulate the number of annual floods that had at least 1 guaranteed image acquisition by a given satellite. For missions that have simultaneous twin satellites in orbit (e.g., Sentinel-1 and 2), images from both satellites were considered. Although there was overlap of Landsat 5 TM and Landsat 7 ETM + acquisition timelines during 1999 and 2012, we only use Landsat 5 TM between 1985 and April 2012. The image gaps created due to the scanline failure in Landsat 7 ETM+ and the impact on image useability are discussed in Methods. Flood events between May 2012 and April 2013 were tested for guaranteed image availability with Landsat 7 ETM+ and from May 2013 until the most recent flood in the database in 2021 by Landsat-8. Flood events occurring after October 2014, and June 2015 were analyzed by Sentinel-1 and Sentinel-2 constellations respectively. Additional information on satellite data availability timelines is presented in Table 1 in the Methodology section.

Acquiring well-timed imagery during a flood is necessary to derive the needed flood information (e.g., extent, depth). However, the presence of frequent and persistent clouds can compromise optical imagery. We therefore investigated the constraints of acquired imagery for the potential for flood detection based on these satellites. Figure 2a provides the annual variability of acquired imagery. Each color is representative of a satellite mission; the envelope represents the number of annual flood events for which at least 1 guaranteed image was available constrained within the upper and lower limit based on cloud cover conditions. The upper limit represents the number of events that had at least 1 image regardless of image quality (i.e., no filtration for clouds). The lower limit of a given colored envelope represents the number of floods that could have been observed after filtration for clouds was performed (≤20% cloud cover; refer to Methodology for details on the rationale for thresholding). These are the number of events that had high-quality imagery. For example, in 2006, the number of events seen by all satellites regardless of image quality is 48. With at least 1 good-quality image (lower limit), there are 18. Some users may be more restrictive when cloud cover is concerned: discarding more images, thus resulting in the true number of useful images being closer to the bottom of the envelope in Fig. 2a. Others may tolerate more cloud cover, which would push image availability toward the upper limit of the envelope.

Table 1 Imagery Search Time Windows for the different satellites on Google Earth Engine.

Sensor	Flood Dates
Landsat 5 TM	From 1985/01-2012/4/30
Landsat 7 ETM+	2012/05/01-2013/4/30
Landsat 8 OLI	2013/05/01-until present day
*Sentinel-1	2014/10/04-until present day
Sentinel-2	2015/06/23-until present day

*Copernicus Sentinel-1B experienced an anomaly on 23 December 2021 related to the instrument electronics power supply provided by the satellite platform, leaving it unable to deliver radar data. Sentinel-1C is targeted for launch in the second quarter of 2023[48]. However, impact on analysis was minimal as (a) revisit periods were calculated between 01/01/2016 and 12/31/2020, and (b) the DFO database used for this analysis contained floods only until 10 September 2021.

The evolution in the number of events with viable imagery through the years provides an understanding of the marginal gain in flood detection as more satellites are added to the existing constellation. We observe a strong increase in the number of detected floods post-2014 (Fig. 2a); this is the timeline marker coinciding with the launch of the Sentinel suite of satellites (Sentinel-1A– April, 2014; Sentinel-2A– June, 2015). More importantly, the number of events with imagery quickly approached the total number of floods, which is more visible in relative numbers, and when the total number of detected events per year is normalized by the total number of floods occurring in the year. The relative number of detected events per year is shown in Fig. 2b.

When the gain in having a guaranteed image regardless of cloud cover for the pre- and post- 2014 eras is quantified, we find an increase from 17% to 84% of DFO events, post-2014. Prior to 2014, only Landsat existed, and as such the 17% is entirely attributed to Landsat. It is interesting to note that, of the 84% post-2014 coverage, 42% of events had a guaranteed acquisition by Landsat-8, rather than an expected value closer to 17% as for the pre- 2014 era. The transition between two eras (pre- 2014 and post- 2014) has seen an increase in Landsat acquisitions. Investigation into durations of floods recorded in the DFO database shows that the average annual duration of a flood before the 2014 era was 9.7 days, and after 2014, 10.0 days: flood duration was fairly constant between the two eras and increased flood duration is not the cause for the increased number of events observed by Landsat. Subsequent investigations revealed that improvement of acquisitions is due to the different number of scenes acquired by the Landsat satellites throughout time. Landsat-5 acquisitions peaked at 147 scenes/day in 1986 and averaged 50–140 scenes/day from 1993 onward. Landsat 7 acquired 438 scenes per day. Landsat 8 has been regularly acquiring 725 scenes per day[22].

An evaluation of the amount of viable imagery (imagery with ≤20% cloud cover) shows that pre-2014, viable imagery by any sensor stood at 7.0% (297 of 4215 events) and increased to 65.8% (602 of 915 events) after 2014. Of this 65.8% we quantify a 56.1% contribution from the Sentinel suite alone (events observed by Sentinel-1, 2 or both, but not Landsat). Events with viable Landsat imagery are at 7.0% and increased to 9.7% post-2014.

Taking into consideration the varying number of global floods that occur annually and potential temporal changes to the sampling provided by the DFO annual flood record (earlier events may be less documented than current ones)[23–25], we normalize the number of floods with images by the total number of floods occurring annually (yellow envelope constrained by two curves in Fig. 2b). The number of events without images normalized by the number of floods in the year are shown as the purple envelope constrained by two curves. As in Fig. 2a, the intervals in 2b represent different levels of user tolerance for

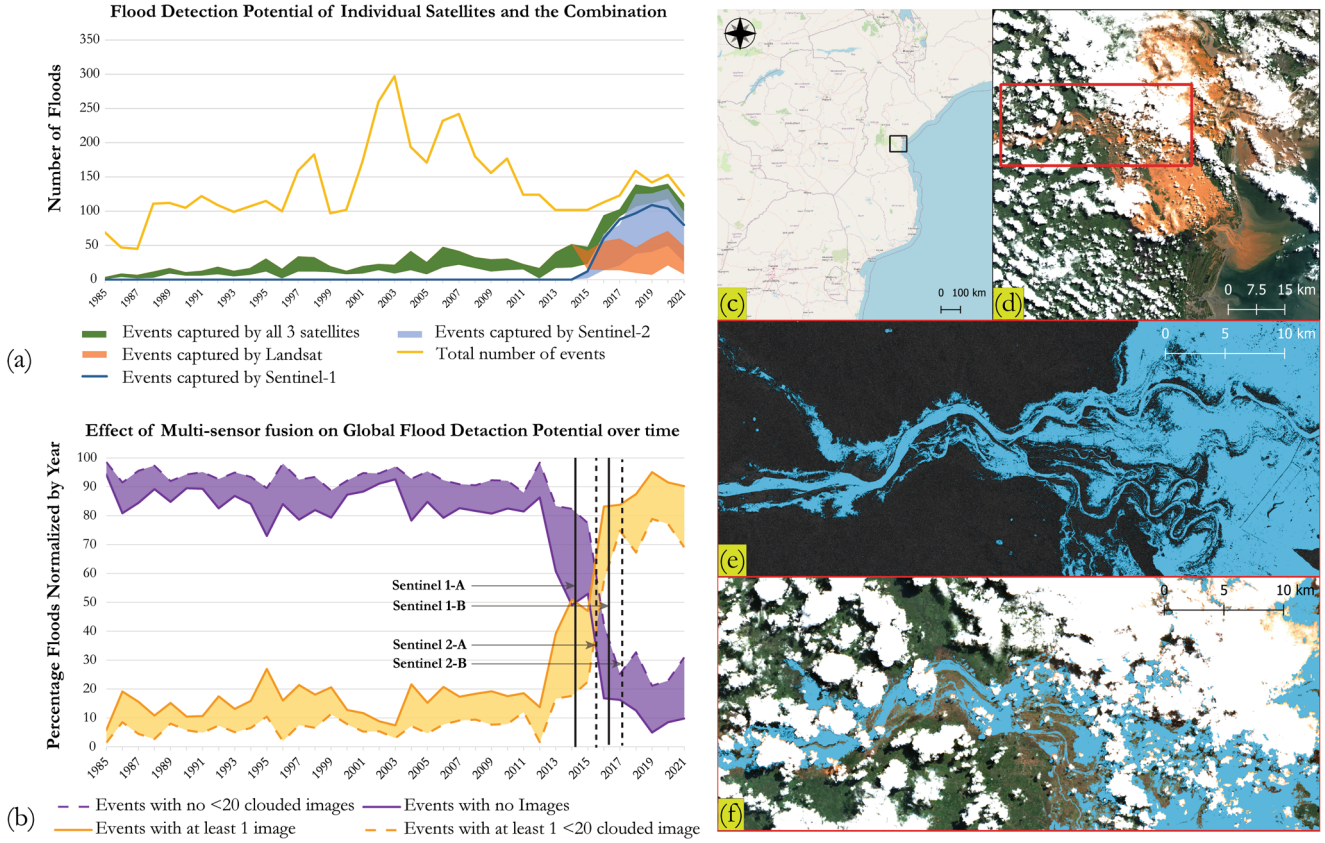

Fig. 2 The benefits of multi-sensor combination for flood detection. a Flood detection potential of individual sensors and gain of detection over time. The orange envelope is overshadowed by the green as prior to Sentinel-1 and 2, events captured by all 3 missions were, in principle, events captured by Landsat. **b** Efficacy of multi-sensor combination in flood detection. The flexibility for the user to choose imagery based on cloud cover is denoted by the yellow envelope, users with higher tolerance to cloud cover expect a fraction of events closer to the upper limit of the envelope, users that require nearly cloud free images expect values closer to the lower limit of the envelope. **c** Beira City, Mozambique where Tropical Cyclone Idai made landfall on March 14, 2019. Base layer credits to QGIS. **d** A near-real time, natural color Sentinel-2 image acquisition of the Beira City flooding. **e**, **f** The impact of cloud cover on image viability illustrated by comparison of near-real time image acquisitions between a Radar (Sentinel-1; E) and optical (Sentinel-2; F) platform. Satellite-captured floodwater is represented by cyan in both panels. Sentinel-2 image credits: Copernicus Sentinel data (2019), processed by ESA, CC BY-SA 3.0 IGO.

cloud cover, with the dashed and solid curves determining the limits for cloud cover (stringent cloud cover filter, dashed yellow line) for the ≤20%; no cloud cover filter (solid yellow line).

We see that the fraction of floods with available imagery, measured as the average of datapoints on the solid yellow line in Fig. 2b increased from 17.7% before 2014 to 82.6 after 2014. For more stringent cases, where potential users may require reduced cloud cover, the availability of viable images before and after 2014 increased from 7.2% to 63.9% (Fig. 2b; average of data points connecting the dashed yellow line before and after 2014). The ratio of the viability of an image per guaranteed acquired image during a flood increased from 0.42 pre-2014 to 0.78 post-2014. This is mostly attributed to the Sentinel-1 radar satellites where cloud interference is minimal.

Figure 2c–f illustrates the significance of multi-sensor combination and the impact of radar platforms. Tropical Cyclone Idai made landfall in Beira city, Mozambique on March 14, 2019 and caused catastrophic flooding that displaced 95,388 people in 19,660 households[26]. The floods mapped using Sentinel-2b (optical) and Sentinel-1b (radar) over the same region only 3 days apart demonstrates (a) the severity of cloud cover affecting the optical sensors, (b) the advantage of the radar acquisition, (c) the need for complementing optical data with radar, and (d) the importance of setting cloud cover thresholds in evaluating image availability for flood studies.

Utility of increased flood detection. Now we investigate how the increase in flood detection potential could be used to analyze floods caused by different drivers over the years. Since the imagery acquired during a flood needs to be of operational use (e.g., to map extent of floods), we only account for the number of viable images (≤20% clouds) available for each of the identified flood drivers. Figure 3a shows that before 2014, when only Landsat was operational, only viable imagery to investigate damages from floods due to snow melt existed at best. There was no usable imagery for extra-tropical cyclones and tidal surges.

Post- 2014 (Fig. 3b), we could observe floods of the following causes using the combination of sensors, with percentages recorded within brackets: Torrential Rains (50%), Others (i.e., Avalanches, Glacial Lake outburst; 50%), Dam/Levee Breaks (55.6%), Tropical Storms (62.4%), Heavy Rains (72,8%), Monsoonal Rains (73%), Snowmelts (80%), Ice jam or ice break-ups (83.3%), Tidal Surges (100%), and Tropical Cyclones (100%). However, no extra-tropical cyclones were captured because none were recorded in the DFO database since 2008 and the 19 that were recorded before 2008 were not captured by Landsat. Thus, there are significant percentage gains of different drivers of flood events when sensor combination is performed: Torrential Rains (46.4%), Others (45.8%), Dam Break/Levee Breaks (43.9%), Tropical Storms (51.8%), Heavy Rains (65.1%), Monsoonal Rains (64.4%), Snowmelt (65.8%), Ice jam or ice break-ups (73.7%),

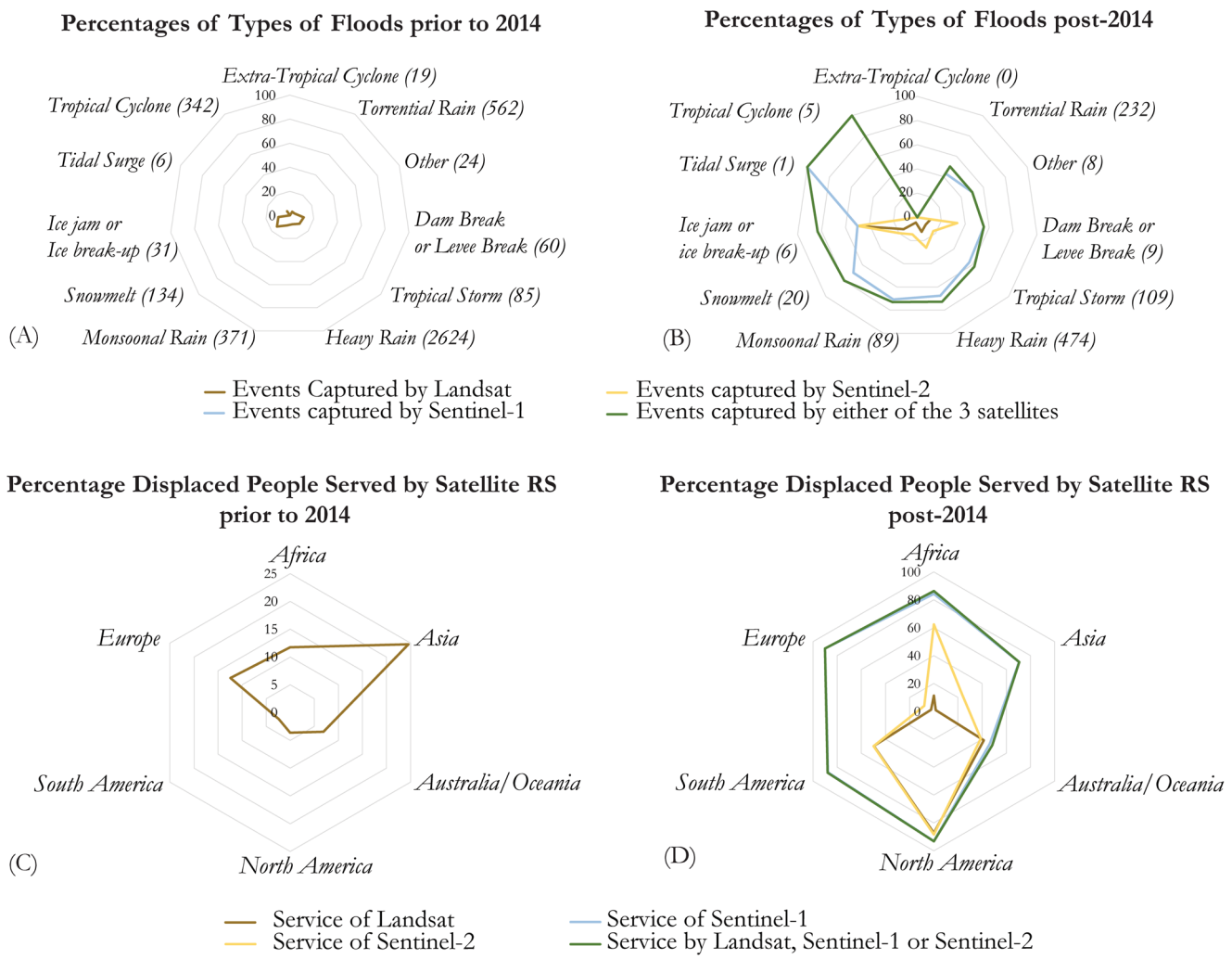

Fig. 3 Comparison of the drivers of floods and differences in human populations served with(out) multi-sensor combination. a Drivers of floods pre-2014 only when Landsat was operational. **b** Drivers of floods post-2014 (Landsat, Sentienl-1 and 2 operational). **c** Displaced population served when only Landsat was operational. **d** Displaced population served with all 3 missions operational.

Tidal Surges (100%), and Tropical Cyclones (95.9%). Further analysis that disentangles the roles temporal sampling, flood duration, and quality control on the availability of viable imagery for each of the flood drivers is located in the supplementary information. It is important to acknowledge that the DFO database is a curated collection of global flood events and has been known to offer an incomplete picture of floods in the African Continent. This is mainly because DFO flood records are often derived from media reports[23,25] and small-scale events or events in remote areas might not be captured by media outlets.

We also assess the societal benefits of multi-mission merging by using the number of people displaced by floods as a proxy for the socioeconomic damage they caused. Greater numbers of viable imagery from medium to high-resolution satellite platforms are desirable for flood impact mitigation. More specifically, imagery made available during the event can be used to assess damage and prioritize and coordinate response. Imagery captured during the flood but made available after the event can be used for surveying damage, coordination of recovery, assessing flood vulnerability, and planning flood resilience measures. In the absence of high-resolution imagery, damage surveying relies on labor and resource-intensive alternatives, such as local surveys of high water marks and aerial (manned or unmanned) imagery.

Of all floods that occurred pre-2014 when only Landsat existed (Fig. 3c), the highest number of displaced people that the Landsat platform could serve was for events in Asia (25% of events had at least 1 viable image). The percentage of events that had at least 1 image in period 2 when considering the combination of data collected by the three satellite missions (Fig. 3d) showed increases in percentual points as follows: Africa (24.4%), Asia (46.2%), Australia/Oceania (41.6%), North America (89.5%), South America (85.4%), Europe (77.6%). The results show that one optical sensor alone had limited reach as a source of high-resolution imagery. However, data provided by a potential multi-mission merger are much more reliable for measuring the flood impacts on populations.

Sentinel-1 radar imagery strongly influences the results due to: (a) the relatively short repeat cycle of Sentinel-1 in comparison to Landsat (6 days vs 16 days) and (b) the reduction in usable optical imagery by clouds. However, optical imagery does help overcome some inherent problems in radar. These include misclassification of surface water in urban areas (urban features misrepresented as water) due to the double bounce phenomenon of the radar beam[27] and wet soils misclassified as water due to backscatter similarities between wet soil and water pixels, or smooth tarmac/asphalt surfaces misclassified due to the specular reflection as with flooded surfaces. Radar imagery is also prone to speckle

noise due to the coherent nature of the radar backscatter[28]. This can result in degraded image quality and make interpretation more difficult[29]. Thus, optical platforms not only complement radar acquisitions through their different orbit cycles, but can also help interpret the radar-derived inundation maps and can be used to provide water quality metrics (e.g., sediment load) of flood water.

Discussion

This study offers several unique findings. Firstly, it provides a quantitative understanding of the role of temporal sampling enabled by individual satellites and their combination in their ability to reliably collect imagery during flood events. Previous studies showed that if a satellite provides an average global revisit time of 2 days, almost all events in Europe could be mapped[7]. While no individual satellite at approximately these spatial resolutions can provide such revisit period for the whole globe, we find that the global average revisit time for the composite 3 satellite missions to be 2.4 days. Moreover, our results complement the body of literature that indicate theoretical coverage based on planned satellite orbits, because we provide here the first measure of the effective revisit time for an ensemble of satellite-mounted sensors. Such may differ from theoretical values due to data availability limitations caused by operational constrains, e.g. spacecraft maneuvers interrupting data acquisition, downlink bandwidth limitations, and others, as well as environmental factors that may impact data quality (in the present case, the inability to directly observe flooded surfaces due to cloud cover). Whereas a global average revisit period of 2.4 days provides a great extension in the ability to survey the flood events such as recorded by the DFO, additional satellites soon to enter operation will undoubtedly improve the potential revisit time.

Two significant additions to the current fleet of satellites capable of surveying surface waters are the SWOT and NISAR missions. The SWOT satellite mission[8,30,31] was launched in December 2022 and will contribute to monitoring of global flood dynamics by providing the first simultaneous measurements of inundation areas and water surface elevation from space, which are very relevant measurements for flood mapping and damage assessment. Also, the NISAR interferometric radar satellite mission, planned for launch in 2024, will provide bi-weekly observations that complement optical data with its cloud penetration capabilities[32] and is therefore expected to provide valuable information for flood responders.

Secondly, we provide two estimates: a conservative and also an optimistic estimate, of how many flood events could be observed by satellites, and of those, how many would have had viable imagery for flood mapping. Thirdly, we provide an overview of the detectability of floods categorized by their causes across the globe by different sensors and their combinations, and the reasons for certain drivers of floods to generate events that can be more easily captured than the others. The breakdown of the needed temporal sampling for floods for each of the different drivers reveals bottlenecks in the current, and possibly future Earth observing systems. It shows, for example, that although the combined sampling is sufficient to capture 90% of the large floods, it is still overwhelmingly lacking in the ability to observe floods caused by extra-tropical cyclones and is insufficient to map floods caused by torrential rains, dam or levee breaks, and others (Fig. 3c). The breakdown by continent also shows potential geographic gaps in the observational network, which is important to prevent biases in studies that use remote sensing observations to characterize floods and relate flood characteristics to driving environmental factors around the globe. For example, see Fig. 3d which shows that floods happening in Australia and Oceania and Asia have a much smaller probability of detection than those in Africa, Europe, North America, and South America. It is important to note that the estimate of flood events with viable imagery in Africa may be overly optimistic due to potential biases in the DFO recording of African floods. Because media reports were an important source of information when creating database entries in the early years of the DFO database, older, smaller events or those happening in remote locations may be overlooked.

With their fine to medium spatial and high temporal resolutions, these satellites, particularly when coupled, will have great potential to improve on the number of floods that are imaged by spaceborne sensors and to generate rapid information of the affected flooded parcels: data that is key to support local government bodies during and after an emergency. Identification of flood extents at different points in time helps identify the extent of the event on a large scale. It also aids in detecting affected infrastructure (i.e., roads and settlements) and impaired regions of interest such as agricultural areas, where flood observation is notoriously sparse. This information can also be used by disaster management agencies and other stakeholders to coordinate appropriate recovery activities, validate insurance claims, and implement effective flood mitigation measures. In addition, having imagery at multiple points during a flood (i.e., rising limb, peak, falling limb) can help validate flood forecasting models such as those currently being employed operationally in the U.S. and elsewhere. These models are also used in simulating floods with different return periods to (a) run damage-impact assessment tests, and (b) guide relocation of residents in flood-prone regions in anticipation of possible upcoming flood events.

The scientific and societal benefits of merging flood data streams from different sensors are evident. The technical and processing methodologies to accomplish this are still to be accomplished. Therefore, future work devoted to identifying and characterizing the exact societal benefits from merging the new and next generation of high-resolution sensors is imperative to transforming the significant potential benefits outlined here into reality. Specific research disciplines that can benefit are the study of flood retention periods on floodplains, flood propagation dynamics, impacts of levees holding or failing[33], and coastal flooding (especially relevant to marginalized populations in the world's deltas[34,35]. However, the amount of data generated will require the development of smart and targeted search queries on very large data cubes and also sophisticated online Big Data processing APIs in order to turn these data into quick actionable information. Merged data can also suffer from potential artifacts that can arise with data from different platforms and their distinct image characteristics, performance, and resolution. Such artifacts can lead to inconsistency in products based on which data source is used for the imaging of an event: a hurdle that can discourage potential users from relying on multi-mission merged products. Thus, additional work is also needed to evaluate the occurrence of such drawbacks and investigate ways to mitigate their deleterious effects. Multi-sensor combination, overall, is an exciting avenue for future research, especially with open data policies now allowing new endeavors in high-frequency flood monitoring.

Methodology

The choice of satellites. For this study, we use Landsat, Sentinel-1 A/B, and Sentinel-2 A/B satellite data. The choice of satellites is driven by their free public availability, temporal span and proven application in surveying water and flood extent dynamics. The Landsat archive contains 40+ years of systematically acquired global optical data. The following Landsat archives on Google Earth Engine (GEE) were used in the study: Landsat 8 OLI

(LANDSAT/LC08/C02/T1_TOA), Landsat 7 ETM+ (LANDSAT/LE07/C02/T1_TOA), Landsat 5 TM (LANDSAT/LT05/C02/T1_TOA).

It is of importance to note that, although Landsat 5 TM and Landsat 7 ETM+ overlapped from 1999 to 2012, we only use Landsat 5 TM between 1984 and April 2012. This is primarily because the Scan Line Corrector (SLC) of Landsat ETM+ failed in 2003, creating a systematic error on image pixels resulting in these scenes being not readily available (uniform stripes of data gaps) in flood mapping applications, with as much as 22% of area per scene being affected by the SLC failure[36]. Therefore, we only use Landsat ETM+ minimally in the analysis when no other Landsat platforms were available (see Table 1 for details).

The launch of the Sentinel-1 satellites in 2014 and 2016 provided free access to global time series data streams to otherwise proprietary radar imagery[37,38], and has been used at different scales for flood mapping since[39,40]. The Sentinel-1 mission consists of a constellation of two polar-orbiting satellites (i.e., Sentinel-1 A/B; Sentinel-1B's data is unavailable since 23 December 2021, Sentinel-1C is planned to take its place) providing C-band synthetic aperture radar imaging, enabling them to gather data in any weather[41]. The following Sentinel-1 archive on GEE was used: COPERNICUS/S1_GRD.

The choice of the Sentinel-2 satellites for this study's flood analysis was based on native resolution: commensurate with Sentinel-1 and Landsat. The Mean Local Solar Time (MLST) at the descending node of Sentinel-2 is 10:30 (am)[41]. This value is close to the local overpass time of Landsat and allows the integration of Sentinel-2 data with existing and historical Landsat missions which consequently aids in long-term high-density time series data collection[41]. The Sentinel-2 mission consists of two polar-orbiting satellites providing optical imaging[41]. The following Sentinel-2 archive on GEE was used: COPERNICUS/S2.

We do not use MODIS (MODerate resolution Imaging Spectroradiometer; onboard Terra and Aqua satellites) data in our analyses as the native resolution of MODIS is an order of magnitude coarser than that of the Landsat and the Sentinel suite. Although MODIS can be useful in providing synoptic views of flood events that might otherwise not be possible with other high-resolution, low spatial coverage sensors, the limited spatial resolution of MODIS hinders the mapping of small-scale floods. Additionally, it is of limited use as a source of validation for hydraulic flood models, even those capable of operating in large domains, such as the LISFLOOD-FP model[42,43], recently used to produce flood risk assessments at 30 m resolution at the scale of the continental United States[44]. While a set of high-resolution imagery obtained during a given flood event can be potentially used to downscale MODIS data, possibly leading to a dense time series of images at the MODIS temporal cadence with the desired spatial resolution to calibrate flood models, such efforts still hinge on the availability of some high-resolution imagery during the flood event. Therefore, we ultimately chose to not use MODIS in the present evaluation.

Calculation of global revisit periods. We estimated the revisit periods, here defined as the average time between two consecutive observations of a particular point on the surface, for the satellite missions Landsat, Sentinel-2 and Sentinel-1 based on a 0.5-degree resolution grid. The grid was created using ArcMap 10.8.1 and intersections of the grid were used to create points. The spacing of land grid points was set to be small enough to capture overlap between satellite observations along-track and across-track), and large enough to manage data processing times (significant overlap of satellite ground tracks at the poles could increase data processing of closely spaced points by orders of magnitude). For each individual point, average revisit times (i.e., to account for irregular revisits, downlink issues) were calculated for each individual satellite and the composite of the three satellites. Averaged revisit times for each of these points were calculated based on the number of image tiles that intersected a particular grid point with more than a 30-minute time difference between each other acquired between 01 Jan 2016 and 31 Dec 2020. This was done to ensure that two image tiles overlapping each other over a point captured at the same time are not double-counted. We only consider revisits between 82.5 N and 55 S of land grid points; Antarctica is omitted from analysis.

$$\text{Average revisit time for a grid point} = \frac{\text{Number of days between 01 Jan 2016 and 31 Dec 2020 (1827)}}{\text{Total Number of Images captured}} \quad (1)$$

For satellite missions that consist of two spacecrafts orbiting simultaneously (Sentinel-1 A/B, and Sentinel-2 A/B), images acquired by both satellites were used in the average revisit period calculation for a given grid point. Sum totals of image tiles of all three missions are used to calculate composite point-based revisit times. These point-based revisit times are later converted to rasters for better visualization purposes (Fig. 1a1–a4).

We use a global flood database (Dartmouth Flood Observatory (DFO) database) as the source of flood locations, duration of floods, causes of floods and the socioeconomic impact of floods to demonstrate the strength of combination of satellites for remote sensing-based flood assessments.

The DFO database. The DFO database is a manually curated repository published by the Dartmouth Flood Observatory, Colorado USA[21], containing 5130 global floods between 1985 and 10 Sep 2021. It contains flood information (i.e., Latitude/Longitude of centroid of flood polygon, number of people displaced, cause of flood, start/end day of flood). We use this database to:

Extract durations of floods to facilitate comparison between average satellite revisit periods. For each flood in the database, image tiles falling within the duration of the flood were enumerated (and consequently subjected to statistical analyses) for the Landsat (Landsat TM, ETM+ and OLI), Sentinel-2 and Sentinel-1 archives separately, by intersecting the centroid of the flood polygon and the satellite image tiles collected within the duration of each flood to detect presence/absence of imagery. Results are presented in Fig. 1b1–b4.

The calculation of average revisit times in the section above has implications when comparing with individual duration of flood events. Individual events in Fig. 1b1–b4 that are guaranteed to be seen might not be seen due to potential clustering. However, on aggregate, when considering a large number of floods on a global scale, individual floods that might be labeled as observed could be missed, or floods that are labeled as missed could be observed because of this clustering effect. Therefore, this is unlikely to change the magnitude of the fraction of floods detected by any individual sensor. We emphasize that the goal of Fig. 1 is to represent the utility of multi-sensor combination in observing global floods over any individual sensor and visualize how the fraction of floods with a guaranteed image increases as sensors are combined.

Comparison between the difference in the detectable drivers of floods during different satellite eras. One of the attributes in the DFO database is the cause of each flood event. Following the literature[14] we break the main cause of flooding recorded in the database into the following 11 unique categories: Extra-Tropical

Cyclones, Torrential Rains, Other (Avalanche Related, Tsunami-related, Glacial Lake Outbursts), Dam Break or Levee Break, Tropical Storm, Heavy Rain, Monsoonal Rain, Snowmelt, Ice jam or ice break-up, Tidal Surge, Tropical Cyclone. A comparison in flood detectability is made for each of the drivers between the pre −2014 era (when only Landsat existed) and post- 2014 (when Landsat and Sentinel missions exist).

We calculate the presence or absence of viable images (<20% cloud cover) that existed for the duration of each of these flood events and break them down by the cause of the flood. We used a maximum cloud cover threshold of 20% as a criterion to identify viable imagery for flood mapping[45]. We compare two distinct time periods; (a) When only Landsat satellites existed, and (b) when other satellites are operational in addition to Landsat. We contrast the differences in the events that are detectable by the combination of these sensors. Note that a flood detected by a satellite could mean that in addition to being detected by that particular satellite there is a possibility for it to be observed by other satellite platforms as well. Results are presented in Fig. 3a/b.

Understanding the societal impact of combination of sensors. The number of people displaced by each flood event is used as a proxy for the socioeconomic impact of flooding. We calculate the presence/absence of viable images (<20% clouds) that existed for the duration of each flood for the different satellite platforms and their combination. We then select floods that had at least 1 viable image and quantify the number of people displaced by each flood according to world's continents. The analysis is performed for two eras; before and after the year 2014 (which roughly coincides with the operationalization of the Sentinel suite of satellites. S1-A and S2-A data acquisition began in April 2014 and July 2015, respectively[38]. Results are presented in Fig. 3c/d.

Data availability

The satellite imagery of Landsat 5 TM, 7 ETM + , 8 OLI, Sentinel-1, and Sentinel-2 used in the analyses can be found in the Google Earth Engine data catalog via the following links respectively: https://developers.google.com/earth-engine/datasets/catalog/LANDSAT_LT05_C02_T1_TOA, https://developers.google.com/earth-engine/datasets/catalog/LANDSAT_LE07_C02_T1_TOA, https://developers.google.com/earth-engine/datasets/catalog/LANDSAT_LC08_C02_T1_TOA, https://developers.google.com/earth-engine/datasets/catalog/COPERNICUS_S1_GRD, https://developers.google.com/earth-engine/datasets/catalog/COPERNICUS_S2. The version of DFO Flood Database used in this study, and the shapefile containing global revisit periods of individual satellites and their combination is available at: https://zenodo.org/records/8164503[46]. All data used to create charts and graphs in the article are available at: https://figshare.com/articles/dataset/Satellite_Detection_of_Floods_Data_supporting_figures_in_manuscript_titled_A_multi-sensor_approach_for_increased_measurements_of_floods_and_their_societal_impacts_from_space_/24454579[47].

Code availability

The Google Earth Engine code that was used to enumerate imagery for the creation of global revisit periods is available from the corresponding author [D.M.] upon request.

Received: 31 March 2023; Accepted: 20 November 2023;
Published online: 08 December 2023

References

1. Li, C. et al. Increased flooded area and exposure in the White Volta River basin in Western Africa, identified from multi-source remote sensing data. *Sci. Rep.* **12**, 1–13 (2022).
2. Munich-Re. *NatCatSERVICE* https://natcatservice.munichre.com/ (2019).
3. Winsemius, H. C. et al. Global drivers of future river flood risk. *Nat. Clim. Change* **6**, 381–385 (2015).
4. Schumann, G. J. P. & Domeneghetti, A. Exploiting the proliferation of current and future satellite observations of rivers. *Hydrol. Process.* **30**, 2891–2896 (2016).
5. Tellman, B. et al. Satellite imaging indicate increasing proportion of population exposed to floods. *Nature* **596**, 80–86 (2021).
6. UNDRR. https://www.undrr.org/publication/earth-observations-action-systemic-integration-earth-observation-applications-national. (2022).
7. Tarpanelli, A., Mondini, A. C. & Camici, S. Effectiveness of Sentinel-1 and Sentinel-2 for flood detection assessment in Europe. *Nat. Hazards. Earth Syst. Sci.* **22**, 2473–2489 (2022).
8. Alsdorf, D. E., Rodríguez, E. & Lettenmaier, D. P. Measuring surface water from space. *Rev. Geophys.* **45**, RG2002 (2007).
9. Brakenridge, G. R., Nghiem, S. V., Anderson, E. & Mic, R. Orbital microwave measurement of river discharge and ice status. *Water Resourc. Res.* **43**, W04405 (2007).
10. Pavelsky, T. M. et al. Assessing the potential global extent of SWOT river discharge observations. *J. Hydrol.* **519**, 1516–1525 (2014).
11. Gleason, C. J. & Hamdan, A. N. Crossing the (watershed) divide: satellite data and the changing politics of international river basins. *Geogr. J.* **183**, 2–15 (2015).
12. Hirpa, F. A. et al. Upstream satellite remote sensing for river discharge prediction: application to major rivers in South Asia. *Remote Sens. Environ.* **131**, 150–151 (2013).
13. Hossain, F. et al. Proof of concept of an altimeter-based river forecasting system for transboundary flow inside Bangladesh. *IEEE J. Sel. Top. Appl. Earth Observ. Remote Sens.* **7**, 587–601 (2014).
14. Frasson, R. P., Schumann, G., Kettner, A. J., Brakenridge, G. R. & Krajewski, W. F. Will the Surface Water and Ocean Topography (SWOT) mission observe floods? *Geophys. Res. Lett.* **46**, 10435–10445 (2019).
15. Lopez, T. et al. On the use of satellite remote sensing to detect floods and droughts at large scales. *Surv. Geophys.* **41**, 1461–1487 (2020).
16. Sikder, S. et al. A synthetic data set inspired by satellite altimetry and impacts of sampling on global spaceborne Discharge characterization. *Water Resour. Res.* **57**, e2020WR029035 (2021).
17. Tulbure, M. G. et al. Can we detect more ephemeral floods with higher density harmonized Landsat Sentinel 2 data compared to Landsat 8 alone? *ISPRS J. Photogramm. Remote Sens.* **185**, 232–246 (2022).
18. United Nations. Sustainable Development Goal 6 Synthesis Report on Water and Sanitation. https://www.unwater.org/publication_categories /sdg-6-synthesis-report-2018-on-water-and-sanitation/(2018).
19. Ahmad, S. K. et al. A fusion approach for water area classification using visible, near infrared and synthetic aperture radar for South Asian conditions. *IEEE Trans. Geosci. Remote Sens.* **58**, 2471–2480 (2019).
20. Wang, L., Jin, G. & Xiong, X. Flood duration estimation based on multisensor, multitemporal remote sensing: the Sardoba reservoir flood. *J. Earth Sci.* **34**, 868–878 (2023).
21. Brakenridge, G. R. Global active archive of large flood events. Dartmouth Flood Observatory, University of Colorado, USA. http://floodobservatory.colorado.edu/ Archives/ (Accessed 13 January 2022).
22. Markham, B. L. et al. Landsat program. *Compr. Remote Sens.* **1**, 27–90 (2018).
23. Adhikari, P. et al. A Digitized Global Flood Inventory (1998-2008): compilation and preliminary results. *Nat. Hazards* **55**, 405–410 (2010).
24. Kettner, A. J., Brakenridge, G. R., Schumann, G. J.-P. & Shen, X. in *Earth Observation for Flood Applications: Progress and Perspectives* (ed G. J-P. Schumann) 147–164 (Elsevier, 2021).
25. Kundzewicz, Z. W., Pińskwar, I. & Brakenridge, G. R. Large floods in Europe, 1985–2009. *Hydrol. Sci. J.* **58**, 1–7 (2013).
26. IFRC. Mozambique: Tropical Cyclones Idai and Kenneth - Emergency Appeal n° MDRMZ014, Final Report. https://reliefweb.int/report/mozambique/mozambique-tropical-cyclones-idai-and-kenneth-emergency-appeal-ndeg-mdrmz014-final-report (2021).
27. Mason, D. C., Giustarini, L., Garcia-Pintado, J. & Cloke, H. L. Detection of flooded urban areas in high resolution Synthetic Aperture Radar images using double scattering. *Int. J. Appl. Earth Observ. Geoinf.* **28**, 150–159 (2014).
28. Ahmed, M. S., Eldin, E., AbdElkawy, F., & Tarek, M. A. Speckle noise reduction in SAR images using adaptive morphological filter. in *10th International Conference on Intelligent Systems Design and Applications*. (2011).
29. Voigt, S., et al., 2008. Extraction of Flood Masks Using Satellite Based Very High Resolution SAR data for Flood Management and Modelling. in *4th Intern. Symp. on Flood Defence*. (2008).
30. Alsdorf, D., Lettenmaier, D. & Vorosmarty, C. J. The need for global, satellite-based observations of terrestrial surface waters. *EOS, Trans. Am. Geophys. Union* **84**, 274–276 (2003).
31. Biancamaria, S., Lettenmaier, D. P. & Pavelsky, T. M. The SWOT mission and its capabilities for land hydrology. *Surv. Geophys.* **37**, 307–337 (2016).
32. NISAR. NASA-ISRO SAR (NISAR) Mission Science Users' Handbook. NASA Jet Propulsion Laboratory. 261 (2018).

33. Syvitski, J. P. M. & Brakenridge, G. R. Causation and avoidance of catastrophic flooding along the Indus River, Pakistan. *GSA Today* **23**, 4–10 (2013).
34. Brakenridge, G. R. et al. Design with Nature: Causation and avoidance of catastrophic floods in Myanmar. *Earth-Sci. Rev.* **165**, 81–109 (2016).
35. Syvitski, J. P. M. et al. Sinking Deltas due to human activities. *Nat. Geosci.* **2**, 681–686 (2009).
36. USGS. https://www.usgs.gov/landsat-missions/landsat-7?qt-science_support_page_related_con=0#qt-science_support_page_related_con. (Accessed January 2022)
37. Singha, M. et al. Identifying floods and flood-affected paddy rice fields in Bangladesh based on Sentinel-1 imagery and Google Earth Engine. *ISPRS J. Photogramm. Remote Sens.* **166**, 278–293 (2020).
38. Mayer, T. et al. Deep learning approach for Sentinel-1 surface water mapping leveraging Google Earth Engine. *ISPRS Open J. Photogramm. Remote Sens.* **2**, 100005 (2021).
39. Martinis, S., Groth, S., Wieland, M., Knopp, L. & Rättich, M. Towards a global seasonal and permanent reference water product from Sentinel-1/2 data for improved flood mapping. *Remote Sens. Environ.* **278**, 113077 (2022).
40. Uddin, K., Matin, M. A. & Meyer, F. J. Operational flood mapping using multi-temporal Sentinel-1 SAR images: A case study from Bangladesh. *Remote Sens.* **11**, 1581 (2019).
41. ESA. https://sentinels.copernicus.eu/web/sentinel/missions/sentinel-2/satellite-description/orbit (Accessed January 2022)
42. Bates, P. D. & De Roo, A. P. J. A simple raster-based model for flood inundation simulation. *J. Hydrol.* **236**, 54 (2000).
43. Horritt, M. S. & Bates, P. D. Effects of spatial resolution on a raster based model of flood flow. *J. Hydrol.* **253**, 239 (2001).
44. Wing, O. E. J. et al. Estimates of present and future flood risk in the conterminous United States. *Environ. Res. Lett.* **13**, 034023 (2018).
45. Munasinghe, D. et al. Intercomparison of satellite remote sensing-based flood inundation mapping techniques. *JAWRA J. Am. Water Resour. Assoc.* **54**, 834–846 (2018).
46. Munasinghe, D., et al. Global datasets to evaluate a multi-sensor approach for observation of floods (Version 1) [Data set]. Zenodo. (2023).
47. Munasinghe, D., et al. Satellite Detection of Floods: Data supporting figures in manuscript titled "A multi-sensor approach for increased measurements of floods and their societal impacts from space". (Version 1) [Dataset]. Figshare. (2023)
48. ESA. https://www.esa.int/Applications/Observing_the_Earth/Copernicus/Sentinel-1/Mission_ends_for_Copernicus_Sentinel-1B_satellite (Accessed January 2023)

Acknowledgements

We would like to thank Livio Loi (RSS-Hydro) for help provided in creating figures and Nishani Moragoda for assistance in proofreading the document. Landsat 5 TM, Landsat 7 ETM+, Landsat 8 OLI collection courtesy of the U.S. Geological Survey. Sentinel-1, and Sentinel-2 collection courtesy of the European Union's Copernicus Program. A portion of this work was performed at the Jet Propulsion Laboratory, California Institute of Technology, under contract with NASA. © 2023. All rights reserved.

Author contributions

D.M., R.P.M.F., C.H.D., M.B., G.S. and G.R.B. conceptualized the study. D.M. conducted the analysis. C.H.D. acquired funding. D.M., R.P.M.F., C.H.D. and M.B. developed the methodology. R.P.M.F. and C.H.D. administered the project. D.M., R.P.M.F. and C.H.D. prepared the original draft of the manuscript. D.M., R.P.M.F., C.H.D., M.B., G.S. and G.R.B reviewed and edited the manuscript.

Competing interests

The authors declare no competing interests.

Additional information

Supplementary information The online version contains supplementary material available at https://doi.org/10.1038/s43247-023-01129-1.

Correspondence and requests for materials should be addressed to Dinuke Munasinghe.

Peer review information *Communications Earth & Environment* thanks Giorgio Boni, Anaïs Couasnon, Peirong Lin, and David Muñoz for their contribution to the peer review of this work. Primary Handling Editors: Rahim Barzegar and Joe Aslin. A peer review file is available.

Reprints and permission information is available at http://www.nature.com/reprints

Publisher's note Springer Nature remains neutral with regard to jurisdictional claims in published maps and institutional affiliations.